Water confined in nanopores: spontaneous formation of microcavities

John Russo, Simone Melchionna, Francesco De Luca

INFM-SOFT, Department of Physics, University of

Rome La Sapienza, P.le A. Moro 2, 00185 Rome, Italy[*]

Cinzia Casieri

INFM-SOFT, Department of Physics, University of L'Aquila, Via Vetoio, 67010 L'Aquila, Italy

Molecular Dynamics simulations of water confined in nanometer sized, hydrophobic channels show that water forms localized cavities for pore diameter $\gtrsim 2.0\,nm$. The cavities present non-spherical shape and lay preferentially adjacent to the confining wall inducing a peculiar form to the liquid exposed surface. The regime of localized cavitation appears to be correlated with the formation of a vapor layer, as predicted by the Lum-Chandler-Weeks theory, implying partial filling of the pore.

I. INTRODUCTION

Nanotubes [1] are important building blocks of nanocomposite materials and nanomachinery. When immersed in ionic solutions, nanometer-sized pores can be used for the detection and analysis of electrolytes and charged polymers, such as DNA [2], and to understand ion transport and selectivity in biological channels [3]. A full understanding of the phase behavior of confined water is a pre-requisite to interpret adsorption and conductivity data. In particular, experiments and simulations have shown that, for channels of sub-nanometer radius water exhibits an intermittent filling/drying transition resulting from an underlying bi-stable free-energy landscape separated by a thermally activated barrier, a behavior specific to water and not observed in a monoatomic fluid [4, 5]. The switch between empty/filled states upon ion translocation has been advocated as a gating mechanism in passive biological channels [6, 7].

---

[*]Electronic address: simone.melchionna@roma1.infn.it

Cavitation of water under confinement is related to the long-ranged attractive forces exerted by hydrophobic bodies. Two alternative mechanisms have been proposed for explaining the occurrence of these forces: on one hand, the presence of air-filled nanobubbles at the solid surface drives the attraction via a bubble-driven mechanism; on the other hand, long-range correlations in the critical region or near the spinodal line could induce an extended density depletion at the surfaces which results in the attraction [8, 9, 10].

The first line of reasoning relies on the pre-existence of air-filled cavities at the solid surface [11]. However, the mechanism for their stabilization is not fully understood since the Laplace-Young equation prescribes an internal pressure of the order of 10^2 atm for nanometer-sized bubbles [12]. One question pertains how such large internal pressure can sustain stable or metastable cavities, and if these are independently nucleated at the solid, corrugated surface. It has been suggested that line tension can act to stabilize such small cavities [13], by reducing the curvature of the bubble base on the solid surface. As a matter of fact, micron-sized air bubbles are commonly observed in proximity of hydrophobic corrugated surfaces and, in the recent literature, there is growing evidence for the presence of bubbles on corrugated surfaces at the nanoscale. In particular, recent AFM experiments on silicon oxyde wafer surfaces of controlled roughness reported on bubble formation at the solid-water interface [14], while syncrotron x-ray reflectivity measurements reported on a small depletion layer in lieu of localized cavitation [16].

The second interpretation is based on the formation of a vapor layer in contact with the solid surface. Such depletion layer would involve a high entropic cost, growing with the extension of the exposed surface, but compensated by volume-dependent forces arising from molecular reorganization. The Lum-Chandler-Weeks (LCW) theory [17] formulates the hydrophobic effect in microscopic terms based on the competition between interfacial and bulk forces which therefore depend on the solute surface/volume ratio. The molecular mechanism underlying the force balance is commonly ascribed to the distortion of the hydrogen bond network. In particular, for small spherical solutes water arranges in a clathrate structure, while for larger size the ensemble of hydrogen bond vectors, O-H···H, points preferentially towards the solute. Therefore, if the curvature of the embedded body is low, the distortion is large and entropic effects prevail over the enthalpic ones, and vice versa for small solutes.

The cylindrical pore represents an opposite case to the spherical solute, where now the confining surface is concave. However, a similar enthalpic/entropic competition is expected

and should depend on the pore diameter. Thus, a relevant information pertains if, for pore diameter larger than that characteristic of intermittent behavior, the liquid phase is completely stabilized or if some peculiar behavior still takes place. The occurrence of cavitation in water confined by cylindrical pores has been recently discussed in view of understanding the hysteresis involved in capillary evaporation [18].

We report here the results of Molecular Dynamics (MD) simulations undertaken on cylindrical, hydrophobic pores of finite length. In section II the simulation set-up and numerical details are described and in Section III the Molecular Dynamics data are illustrated. In Section IV the LCW theory is described and the numerical solutions are compared with the simulation results. The last Section draws some conclusions and analyzes recent experimental observations.

II. SIMULATION DETAILS

The geometry of the simulation set-up is depicted in Fig. 1. The two pore mouths are connected to the same, periodically folded, reservoir of quasi-bulk water. The pore diameter d and pore length L are varied to the following pairs of values $(d, L) = (1.5, 4.0)$, $(2.0, 4.0)$, $(2.5, 4.0)$, $(2.5, 8.0)$, $(3.0, 4.0)$ and $(3.5, 4.0)\,nm$, as used to label the runs. Simulations become rapidly costly with the pore size and we did not attempt to extend our simulations to larger geometries. Besides the nominal values, the effective cylinder diameter and length were evaluated via the criterion that the repulsive wall-oxygen potential be less than $k_B T$, giving a reduction of the effective diameter and increase of effective length by $0.46\,nm$ [5].

The simulation box is periodic in all three directions with dimensions depending on the pore geometry. The number of water molecules for all simulations ranges between 852 and 2464 units. Water is represented via the SPC/E computational model [22]. The confining oxygen-wall potential is modeled as a smooth surface generated by carbon atoms distributed uniformly over the surface. The wall-water interaction acts between each water oxygen and a smooth Lennard-Jones potential integrated over the dark region of the wall in Fig. 1. Each carbon atom carries a Lennard-Jones potential with parameters $\sigma = 0.345\,nm$ and $\epsilon = 0.7294\,kJmol^{-1}$ [5] and standard Lorentz-Berthelot rules are used to construct oxygen-wall interactions. Electrostatic interactions between charged oxygen and hydrogen atoms are computed with the Ewald method via the Smooth Particle Mesh Ewald implementation

[19]. Moreover, the confining medium is taken as non polarizable.

Special care is taken to keep the reservoir density under control, such that upon emptying/filling of the channel the reservoir maintains a bulk-like behavior with an average mass density of $1\,gr/cm^3$ away from the pore. This is obtained by varying over time the length of the reservoir, in direction parallel to the pore axis, by a Berendsen type of piston [20], with a characteristic coupling time of $10\,ps$, during the equilibration and production runs. The feedback sets the average density in a stripe of thickness $t = 10\,nm$ placed at distance $l = 7\,nm$ away from the pore (see Fig. 1). The system temperature is controlled via a Nosè-Hoover thermostat [21] in order to avoid anomalous temperature drifts during both the equilibration process and the subsequent production runs. The system is simulated at $300\,k$ while some auxiliary simulations are made at 280 and $320\,K$. The evolution of the system is followed over times of $100\,ps$ (equilibration) and, subsequently, of $1\,ns$ (production). Within the simulation time window, stationarity is monitored by following the number of molecules populating the channel and the formation and size distribution of cavities. In order to monitor the effective stationarity of the equilibrated system, the run of the $(2.5, 4.0)\,nm$ geometry has been further extended to $3\,ns$, without observing any departure from stationarity.

In order to detect the cavities we have used a coarse-graining procedure by tesselating the space with cubic cells of edge $0.02\,nm$. An empty cell is defined by having the distance from any oxygen atom greater than $0.3\,nm$. The wall position is defined by the largest radial distance of an oxygen atom from the pore axis and adding an offset of $0.1\,nm$. A cavity is defined as the cluster of contiguous empty cells which do not belong to the wall region. The distinction among clusters is made via a graph algorithm and sorted according to size. In this way, the identity of cavities is clearly established.

III.   MOLECULAR DYNAMICS RESULTS

The simulation data present two distinct behaviors: for the geometries $(1.5, 4.0)\,nm$ at $T = 300\,K$ and $(2.5, 4.0)\,nm$ at $T = 280\,K$ we observe emptying of the pore, with a large vapor region extending between the two pore mouths; on the other hand, for the geometries $(2.0, 4.0)$, $(2.5, 4.0)$, $(2.5, 8.0)$, $(3.0, 4.0)$ and $(3.5, 4.0)\,nm$, water persists inside the pore at density close to liquid state, with formation of nanobubbles in proximity of the confining wall.

At first we report on the process of emptying of the channel, as depicted in Fig. 2. Given an initial, apparently stable liquid inside the channel, a number of distinct lateral cavities are formed in proximity of the cylinder wall. Subsequently, one of such bubbles grows in size, rapidly extending over the whole pore volume. The final state appears to be stable over the $1\,ns$ time scale. The homogeneous growth of the vapor region is consistent with the recently proposed model of capillary evaporation in hydrophobic pores [18].

Intermittent emptying/filling of the channel has been previously reported at $T = 300\,K$ for $d \lesssim 1.5\,nm$ and $L \lesssim 1.0\,nm$ (and eventually for larger diameters at lower temperatures) by using MD simulations with the same computational model as used here [5]. In the previous work, it was found that the time scale of emptying/filling oscillations is of the order of $\sim 100\,ps$. In the current case, the direct observation of intermittency is prohibitive in terms of CPU time. In fact, given the larger pore diameters, intermittency could take place over timescales longer by one order of magnitude, or more [7]. Therefore, we preferred to focus on the interfacial structuring of the liquid in the filled state.

It is interesting to note that the geometry $(2.4, 4.0)\,nm$ exhibits pore emptying for $T = 280\,K$ and pore filling for $T = 300\,K$. The fact that emptying/filling of the pore is sensitive to differences in temperature as small as $\Delta T = 20\,k$ is an indication that the underlying bulk phase diagram, with the rather narrow region of bulk liquid water and the close-by liquid-vapor coexistence, is an important driving factor for the confined fluid.

For the filled channel, the liquid interface displays the patterns shown in Figs. 3 and 4. The interface is rather corrugated by the presence of cavities appearing in proximity of the confining wall (lateral cavities), and rarely observed as spherical shape located around the cylinder axis. The cavities resemble spherical caps or rounded cones, with volumes much larger than the molecular size ($v_w \simeq 0.027\,nm^3$). The average volumes range between $\langle v \rangle / v_w = 5.7$ for the $(d, L) = (2.0, 4.0)\,nm$ geometry and $\langle v \rangle / v_w = 21.0$ for $(d, L) = (3.5, 4.0)\,nm$. The peculiar pattern of the liquid exposed surface is rather representative of the highly cohesive character of water. It should be noticed that the shape of the vapor cavities along the transversal section does not appear to be flattened against the wall, while in the longitudinal direction visual analysis does not allow to draw a clear conclusion. We infer that line tension effects can be important only along the longitudinal direction but not on the transverse direction. In terms of dynamics, the cavities present high mobility with fast reshaping on the $1\,ps$ time scale.

The distribution of cavity size is illustrated in the normalized histograms of Fig. 5. A systematic increase of cavities of larger volume with the pore diameter is visible, accompanied by a depletion of smaller, molecular-sized ones. The distribution becomes more shifted to the right as the diameter of the cylinder grows. In contrast, water in proximity of a planar hydrophobic surface exhibits cavities with reduced volumes, basically indistinguishable from fluctuations of size of the molecular volume v_w.

In fig. 6 we report the same histograms but we filter out the contributions arising from cavities of volume $v < v_w$. By rescaling the abscissa by the cylinder surface area, the histograms become peaked around the same value $v/(v_w \pi dL) \simeq 2\,nm^{-2}$, and width increasing with the pore diameter. However, the integrated cavity volume per unit surface is mostly contributed by the right tails of the distributions, which appear to be equal for the $(2.5, 4.0)$ and $(3.5, 4.0)$ geometries but significantly shifted to the left for the $(1.5, 4.0)$ case. Therefore, cavitation does not seem to grow further as the diameter is larger than $2.5\,nm$.

The longer channel does not appear to affect the histogram, indicating that the bubble formation does not depend on interfacial effects arising from the finite pore length. In principle, the finite length could affect the liquid/vapor balance and the drying transition. In fact, by using an elementary macroscopic argument [12], the difference in free-energy density between the liquid and vapor states is approximated by $\Delta\Omega/\pi dL = \gamma_{lw} - \gamma_{lv}d/2L$ where γ_{lw} and γ_{lv} are the liquid-wall and liquid-vapor surface tensions under ambient conditions, respectively, and bulk contributions to the free energy have been neglected. In other words, if finite channel effects are in place, by making the channel longer, one should move away from the vapor branch. By taking $\gamma_{lw} = 7.4\,k_BT/nm^2$ and $\gamma_{lv} = 26\,k_BT/nm^2$ it is seen that the geometry $(d, L) = (2.5, 4.0)\,nm$ is close to the region where the free-energy difference changes sign [5]. Our simulation at room temperature for $(d, L) = (2.5, 8.0)\,nm$ showed that the channel remains filled as much as the $(2.5, 4.0)\,nm$ geometry, without appreciable differences in the distribution of cavity volumes. Conversely, the sensitivity to the pore length appears in the fluctuations of the number of adsorbed water molecules, which approximately drops by a factor two in the longer channel. We interpret the weak size dependence of cavitation as due to the corrugated, largely exposed surface of the liquid with respect to the simple macroscopic model, that renders finite size effects negligible already at $L = 4\,nm$.

IV.   LUM-CHANDLER-WEEKS PREDICTIONS

In this section we compare our data to the predictions of the LCW theory for an infinitely long pore. Schematically, the theory can described as follows. Let us first consider the decomposition of the microscopic density $n(r)$ into a slowly varying component, $n_s(r)$, and a fast component, $n(r) - n_s(r)$. The LCW theory builds upon the well-known square-gradient theory for liquid-vapor coexistence [25] by taking into account self-consistently the fast oscillations in density. According to the square gradient approximation, the local grand potential $-W(n)$ is related to the laplacian of the density via

$$\left(\frac{dW}{dn}\right) = m\nabla^2 n(r) \tag{1}$$

where m is an effective parameter derived from the underlying interatomic potential $v(r)$, $m = -\frac{\pi}{6}\int_0^\infty dr r^4 v(r)$ (Random Phase Approximation [25]). By applying a coarse graining procedure, the local density is replaced by the function $n \to \bar{n} = n + \frac{\lambda^2}{2}\nabla^2 n$ where λ is the characteristic length of the coarse graining procedure. Therefore, the starting equation of the LCW theory is derived from eq.(1) rewritten in terms of $\bar{n}$, and asserting that this equations holds for the slow component n_s, thus

$$\left(\frac{dW}{dn}\right)_{n_s} = \frac{2m}{\lambda^2}[\bar{n} - n_s] \tag{2}$$

for which we choose $\lambda = 0.3\,nm$ and $m = 919.9 \times 10^{21}\,Jnm^5 mol^{-2}$. To implement eq. (2) one needs prior knowledge of the bulk equation of state of water near the liquid-vapor coexistence. Following previous studies [23], we used a quartic dependence plus a linear correction term which models the proximity to coexistence,

$$W(n) = \alpha\,(n - n_l)^2\,(n - n_g)^2 + \beta(n - n_l) \tag{3}$$

where $\alpha = 2.89 \times 10^{-24}\,Jnm^9$, $\beta = 3.04 \times 10^{-29}J$ and the liquid and vapor densities are $n_l = 32.94\,nm^{-3}$ and $n_g = 7.7 \times 10^{-4}\,nm^{-3}$, respectively [23]. By solving the equations in cylindrical coordinates and forbidding any angular symmetry breaking, we did not attempt to observe the formation of cavities of given shape. This choice was motivated by the narrow range of numerical stability found during the solution of the LCW equations.

The link between the slowly varying and the complete density fields is established within

the gaussian density fluctuations approximation, by writing [24]

$$n(\mathbf{r}) = n_s(\mathbf{r}) - \int d\mathbf{r}' c(\mathbf{r}')\chi(\mathbf{r}, \mathbf{r}') \tag{4}$$

where the response function $\chi(\mathbf{r}, \mathbf{r}') \equiv \langle \delta n(\mathbf{r})\delta n(\mathbf{r}') \rangle$ is approximated by $\chi(\mathbf{r}, \mathbf{r}') \simeq n_s(\mathbf{r})\delta(\mathbf{r} - \mathbf{r}') + n_s(\mathbf{r})n_s(\mathbf{r}')h(|\mathbf{r} - \mathbf{r}'|)$ and $h(|\mathbf{r} - \mathbf{r}'|) - 1$ is the bulk pair correlation function. Moreover, $c(\mathbf{r})$ is the water-wall direct correlation function. Given $n_s(\mathbf{r})$, eq.(4) is solved to obtain $c(\mathbf{r})$ and $n(\mathbf{r})$ via the Nystrom numerical procedure [26]. The two coupled integro-differential equations (2) and (4) are solved iteratively. We did not include the correction to the LCW theory due to the attractive part of the wall-oxygen potential [23]. Vice versa, the effective diameter of MD and the diameter used in LCW calculations, $\bar{d}$, were considered as equivalent control parameters.

We have found that for diameter $\bar{d} < 2.6\,nm$ the LCW equations predict complete pore emptying, in agreement with previous simulation and experimental results, but below our MD data which exhibit emptying (or eventually intermittency) for effective diameter $\lesssim 2.0\,nm$. However, in this geometry the LCW predictions do not distinguish between intermittent and cavitating behavior. In the range $2.6 < \bar{d} < 3.8\,nm$ the theory predicts partial filling of the pore, as illustrated by the density profiles in Fig. 4, where the micro-phase coexistence is accompanied by a significant density depletion near the wall. Moreover, the LCW equations predict a gradual increase of the vapor layer as the diameter lowers, whilst the MD results show a maximum which varies slowly with the pore diameter. Following previous authors [23], we attribute this difference to the presence of the weak attractive tail in the water-wall potential. Finally, at larger diameters, the LCW curves show weakly structured profiles, with a characteristic non-wetting shape near contact. In essence, the LCW theory predicts a cross-over between empty and partially filled states for $\bar{d} = 2.6\,nm$, larger than the MD results where the cross-over appears in the $1.5 : 2.0\,nm$ interval. This discrepancy may be attributed to the one-dimensional solution of the LCW equations and to the missing attractive tail in our theoretical treatment, causes which artificially stabilize the vapor phase, or to the undetermined location of the confining surface, whose diameter can vary by about $0.5\,nm$.

Notwithstanding the negligible correlations emerging from the LCW solutions, we can compare MD and LCW data regarding the number of water molecules filling a channel of length $4\,nm$ as a function of the channel effective diameter $\bar{d}$. From Fig. 8 it is apparent

that the LCW model shows systematically lower values than the MD data in the region where the theory exhibits partial filling. The MD data are intermediate between the LCW values and the simple model of uniform filling of the pore at the water liquid density. As for the discrepancy in the cross-over diameter, the lack of longitudinal symmetry breaking and the weak attractive tail in the simulated water-wall potential, might explain the smaller number of water molecules predicted by the LCW theory.

V. CONCLUSIONS

The behavior of water in contact with an extended hydrophobic surface has attracted considerable attention on account of the intrinsic thermodynamic problem, which has significant implications for protein folding [23], for ionic transport in biological channels [3] and for the boundary conditions for fluid flow in microchannels [28].

Our study clearly demonstrates the spontaneous formation of vapor microcavities on the nanometer scale for water in contact with a concave cylindrical surface of diameter $d \gtrsim 2.0\,nm$. The cavities are localized both in the angular and, more importantly, in the longitudinal directions. To our knowledge, this surprising result is the first observation for water confined in such geometry.

The results are particularly interesting for the on-going debate on the hydrophobic effect, in which a number of different interpretations have been put forward, such as entropic effects due to molecular rearrangement, electrostatic effects and spontaneous cavitation due to the metastability of the fluid [10]. Recent experiments have focused on analyzing water in contact with a hydrophobic surface and found contrasting results. In particular, either cavitation [14, 15] or an extended low-density depletion layer [16] have been observed. The fact that water around a concave, but smooth, hydrophobic surface forms short-ranged islands of vapor, modulated by the surface curvature, suggests that the contrasting experimental observations arise from the sensitive structural response of water to the roughness of the solid surface.

Moreover, our study sheds some light on the experimental observation of hysteresis in water intrusion/extrusion cycles in pores and the interpretation based on homogenous nucleation [18]. The simulation data underline the metastable character of highly confined water. However, the rich structural patterns exhibited by the interface are absent in a sim-

ple fluid and, therefore, are unlikely to be explained in terms of a macroscopic approach. When comparing the simulation data with a quasi-microscopic treatment, namely the Lum-Chandler-Weeks theory, the density profiles and the cross-over diameter between empty and partially filled states of the latter were found to agree only qualitatively with the simulation data. The discrepancies were explained on the basis of the one-dimensional solution of the LCW equations.

Finally, we wish to comment on some recent measurements on ionic conductance in nanopores of diameter $d \simeq 10\,nm$ showing that transport displays an anomalous response, with a five orders of magnitude reduction in the current spectral density power and a strongly noisy response with respect to bulk behavior [29]. This has been attributed to the presence of spherically shaped air bubbles trapped inside the nanopores such that the translocating ions encounter a two-phase filled region. Although the differences in pore diameter between the presently simulated and the experimental systems might seem large, one might expect that water cavitation is still effective in the wider pores or that cavitation is locally enhanced by the translocating ion. The effect of such cavitation would induce non trivial wall-ion dielectric interactions, modulated by the imperfect screening of water, and non trivial hydrodynamic forces. Such scenario would imply a coupled ion-bubble transport mediated by the microscopic liquid-vapor coexistence.

VI.   ACKNOWLEDGEMENTS

Figure Captions

Figure 1: Schematic representation of a cut through the simulation cell. The dark area is the confining cylindrical wall and the shaded area is the region where water is maintained at mass density of $1\,gr/cm^3$ (see text for details).

Figure 2: Snapshots of the $(1.5, 4.0)\,nm$ channel at four different instants separated by $10\,ps$ showing the process of pore emptying. The pictures are produced with the surface generation algorithm of the VMD software [27] by taking into account the oxygen atoms only.

Figure 3: Snapshot of an instantaneous configuration of the $(2.5, 4.0)\,nm$ channel, generated as for Fig.2.

Figure 4: Evolution of cavities (shaded regions) formed in the $(2.5, 4.0)\,nm$ pore at $300\,K$, and analyzed on a slab of thickness $0.1\,nm$ placed at the midpoint of the pore axis. The four snapshots (a,b,c,d) correspond to successive configurations separated by $1\,ps$. The white region corresponds to the wall region, grey to water filled regions, black to the empty regions (see text for details).

Figure 5: Frequency of occurrence of cavities with volume v normalized by the volume per water molecule ($v_w = 0.027\,nm^3$) for (d, L) equal to $(2.0, 4.0)\,nm$ (solid line), $(2.5, 4.0)\,nm$ (dashed line), $(2.5, 8.0)\,nm$ (long dashed line), $(3.5, 4.0)\,nm$ (dot-dashed line) and for water close to an infinite plane (dotted line). All data are at $T = 300\,K$. To highlight the dependence on the pore geometry, the normalized frequency of occurrence $P(v)$ is multiplied by the volume. The inset displays the unscaled frequency (same symbols of the main plot).

Figure 6: Histograms as in Fig. 5, but for cavity volumes larger than v_w . The three curves refer to $(d, L) = (2.0, 4.0)$, $(2.5, 4.0)$ and $(3.5, 4.0)\,nm$, with line styles as in Fig. 5. Abscissa have been divided by the cylinder surface area.

Figure 7: Radial density profiles divided by the density of liquid water n_l. The radial coordinate is rescaled with the effective radius (MD data) and the value $\tilde{d}/2$ (LCW data). Upper panel: MD profiles at $300\,k$ for nominal pore diameter $d = 2.0\,nm$ (black), $2.5\,nm$ (red), $3.0\,nm$ (green) and $3.5\,nm$ (blue) and length $L = 4\,nm$. Middle panel: LCW profiles for $\tilde{d}$ equal to $2.8\,nm$ (black), $3.0\,nm$ (red), $3.4\,nm$ (green), $3.6\,nm$ (blue). Lowner panel: LCW profiles for $\tilde{d}$ equal to $3.8\,nm$ (black), $4.0\,nm$ (red), $6.0\,nm$ (green), $10.0\,nm$ (blue).

Figure 8: Number of water molecules occupying channels of length $4\,nm$ obtained from MD (filled circles), LCW solutions (open squares) and a uniform filling of the channel (dashes curve). The vertical jump in the LCW curve signals the cross-over between empty and partially filled states.

[1] S. Iijima, Nature, 56, 354 (1991).

[2] J.J. Kasianowicz, E. Brandin, D. Branton, D.W. Deamer, *Proc. Natl. Acad. Sci. U.S.A.*, **93**, 13770, (1996).

[3] B.Hille, *Ionic channels of excitable membranes* (Sinauer Associated, Sunderland, MD, 1992).

[4] G. Hummer, J.C. Rasaiah, J.P. Nowortya, *Nature (London)*, **414**, 188 (2001).

[5] R. Allen, S. Melchionna, J-P. Hansen, *Phys.Rev.Lett.*, **89**, 175502 (2002). *J.Chem. Phys.*, **120**, 4927 (2004).

[6] J. Dzubiella, J.-P. Hansen, *J.Chem.Phys.* **122**, 234706 (2005).

[7] O. Beckstein, K. Tai, and M. S. P. Sansom, *J. Am. Chem. Soc.*, **126**, 14694 (2004).

[8] P. Attard, C.P. Ursenbach, G.N. Patey, *Phys. Rev.A*, **45**, 7621 (1992).

[9] D.R. Bérard, P. Attard, G.N. Patey, *J. Phys. Chem.*, **98**, 7236 (1992).

[10] E.E. Meyer, K.J. Rosenberg, J. Israelachvili, *Proc. Natl. Acad. Sci.* USA, 10.1073/pnas.0606422103 (2006).

[11] P. Attard, *Adv. Colloid Interface Sci.*, **104**, 75 (2003).

[12] J.-L. Barrat, J.-P. Hansen, *Basic concepts for simple and complex liquids*, Cambridge University Press (2003).

[13] T. Pompe, S. Herminghaus, *Phys.Rev.Lett.* **85**, 1930 (2000).

[14] J. Yang, H. Duan, D. Fornasiero, J. Ralston, *J.Phys.Chem.B* **107**, 6139 (2003).

[15] N. Ishida, R. Inoue, M. Miyahara, K. Higashitani, *Langmuir*, **16**, 6377 (2000).

[16] A. Poynor, L. Hong, I.K. Robinson, S. Granick, Z.Zhang, P.A. Fenter, *Phys.Rev.Lett.* **97**, 266101 (2006).

[17] K. Lum, D. Chandler, J.D. Weeks, *J. Phys. Chem. B*, **103**, 4570 (1999).

[18] B. Lefevre, A. Saugey, J.-P. Barrat, L. Bocquet, E. Charlaix, P.F. Gobin, and G. Vigier, *J.Chem.Phys.*, **120**, 4927 (2004).

[19] U. Essmann, L. Perera, M.L. Berkowitz, T. Darden, H. Lee, L.G. Pedersen. *J.Chem.Phys.* **103**, 8577 (1995).

[20] H.J.C. Berendsen, J.P.M. Postma, W.F. van Gunsteren, A. Di Nola, J.R. Haak, *J.Chem.Phys.*, **81**, 3684, (1984).

[21] D. Frenkel and B. Smit, *Understanding molecular simulation* (Academic Press, London, 1996).

[22] W.L. Jorgensen, J. Chandrasekhar, J.D. Madura, R.W. Impey, M.L. Klein, *J. Chem. Phys.* **79**, 926 (1983).

[23] D.M. Huang, D. Chandler, *J. Phys. Chem. B*, **106**, 2047 (2002)

[24] D. Chandler, *Phys.Rev. E*, **48**, 2898 (1993)

[25] J.P. Hansen and I.R. McDonald, *Theory of simple liquids*, 3rd edition, Academic Press (2006).

[26] W.H. Press et al., *Numerical Recipes in C: the art of scientific computing*, Cambridge University Press.

[27] W. Humphrey, A. Dalke, K. Schulten, *J. Molec. Graphics*, **14**, pp. 33 (1996).

[28] P.-G. de Gennes, *Langmuir* **18**, 3413 (2002).

[29] R.M.M. Smeets, U.F. Keyser, M.Y. Wu, N.H. Dekker, C. Dekker, *Phys.Rev.Lett.*, **97**, 088101 (2006).
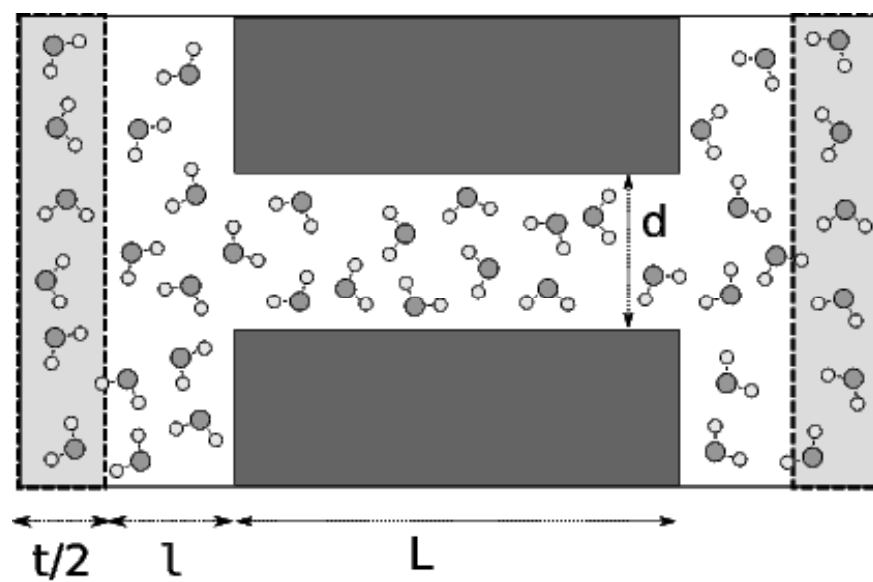
Figure 1, Russo et al.
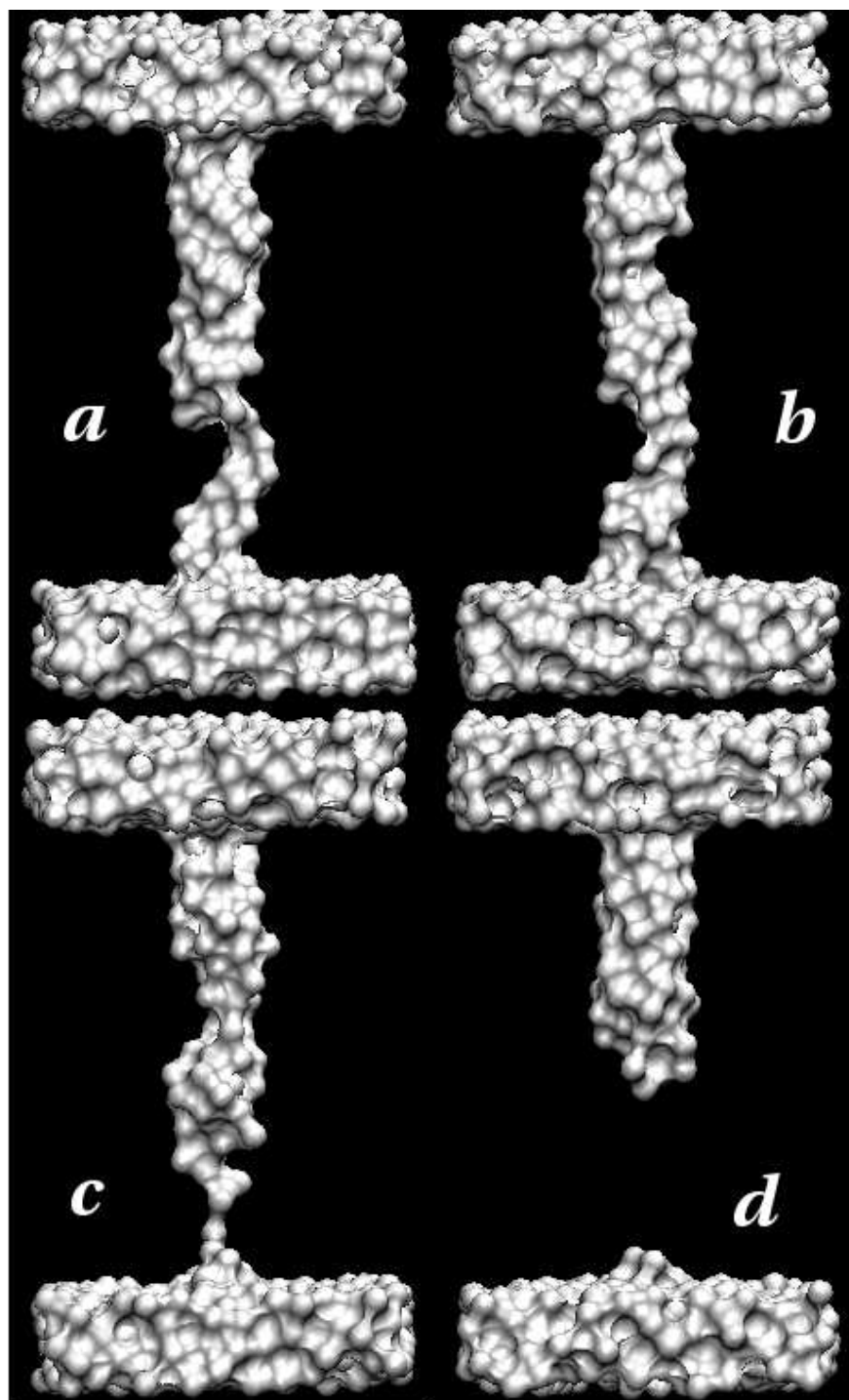
Figure 2, Russo et al.
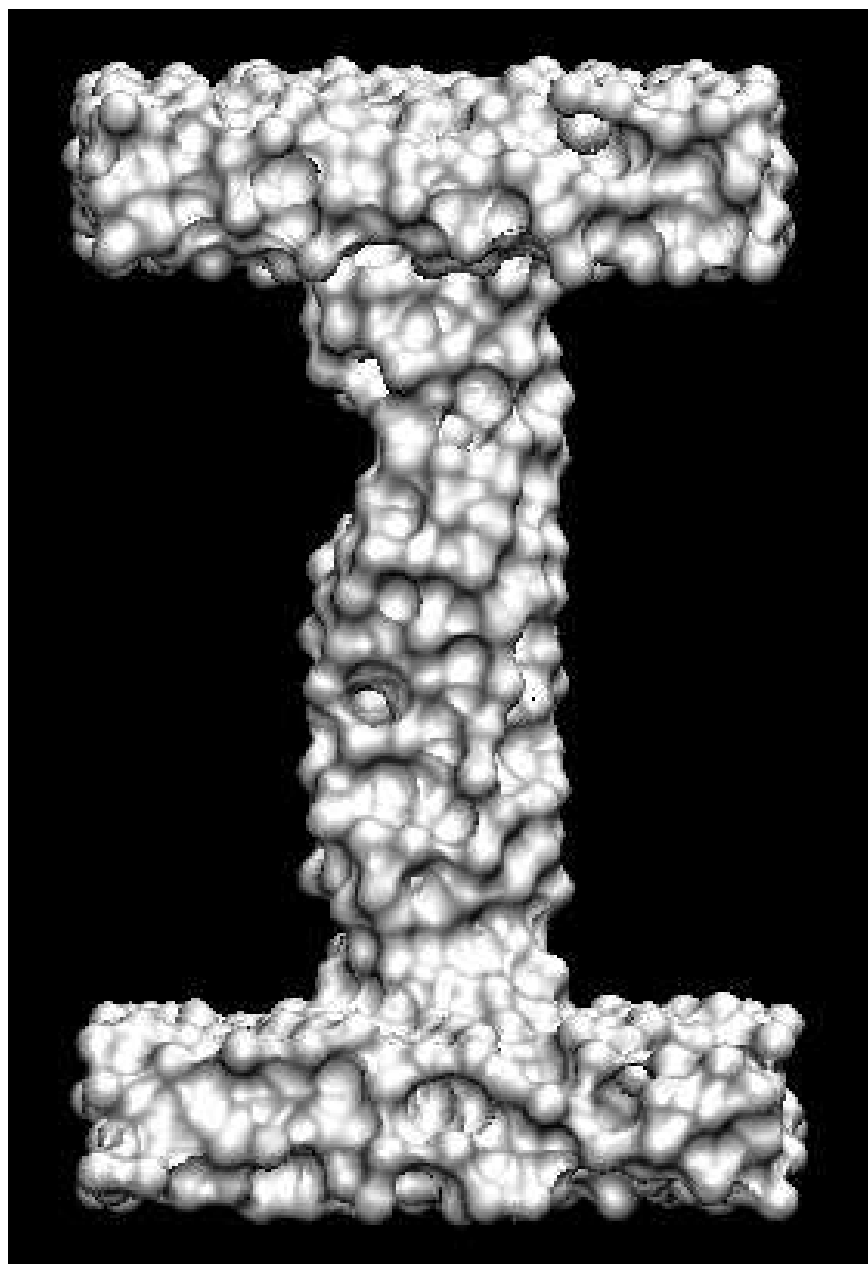
Figure 3, Russo et al.
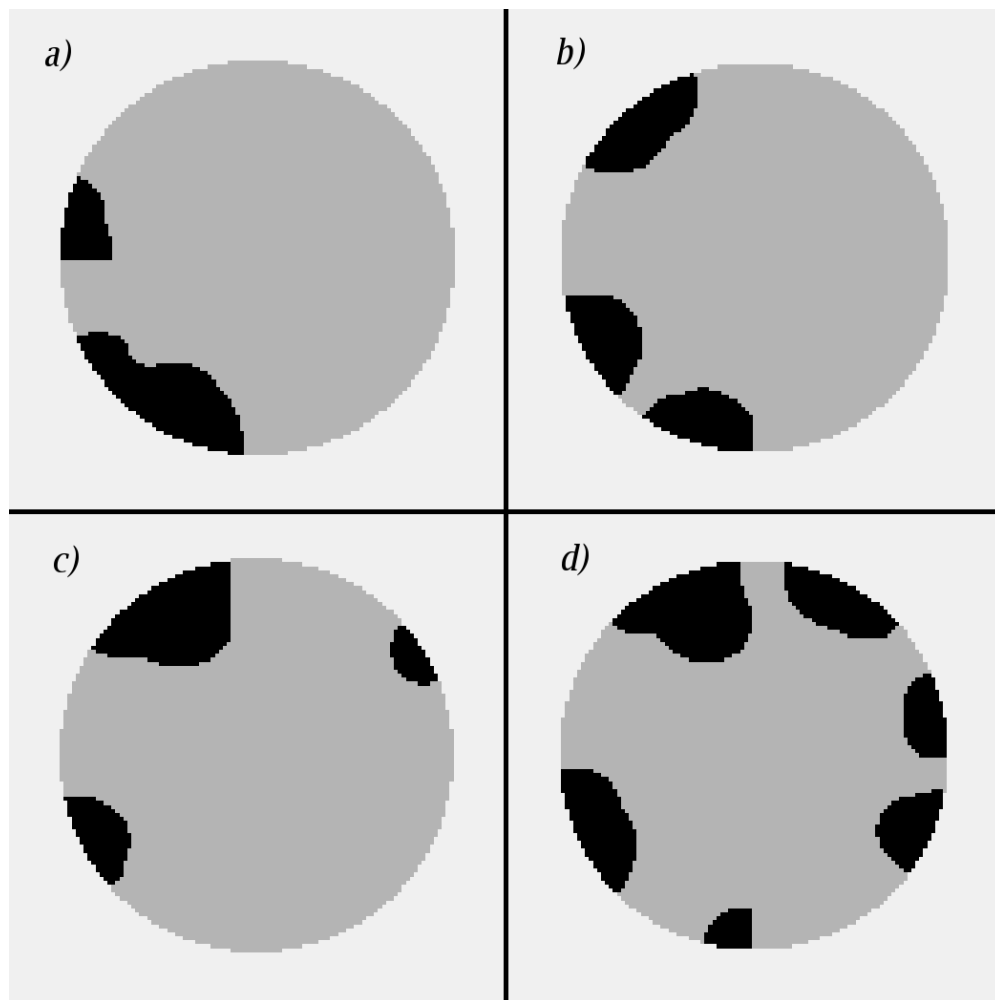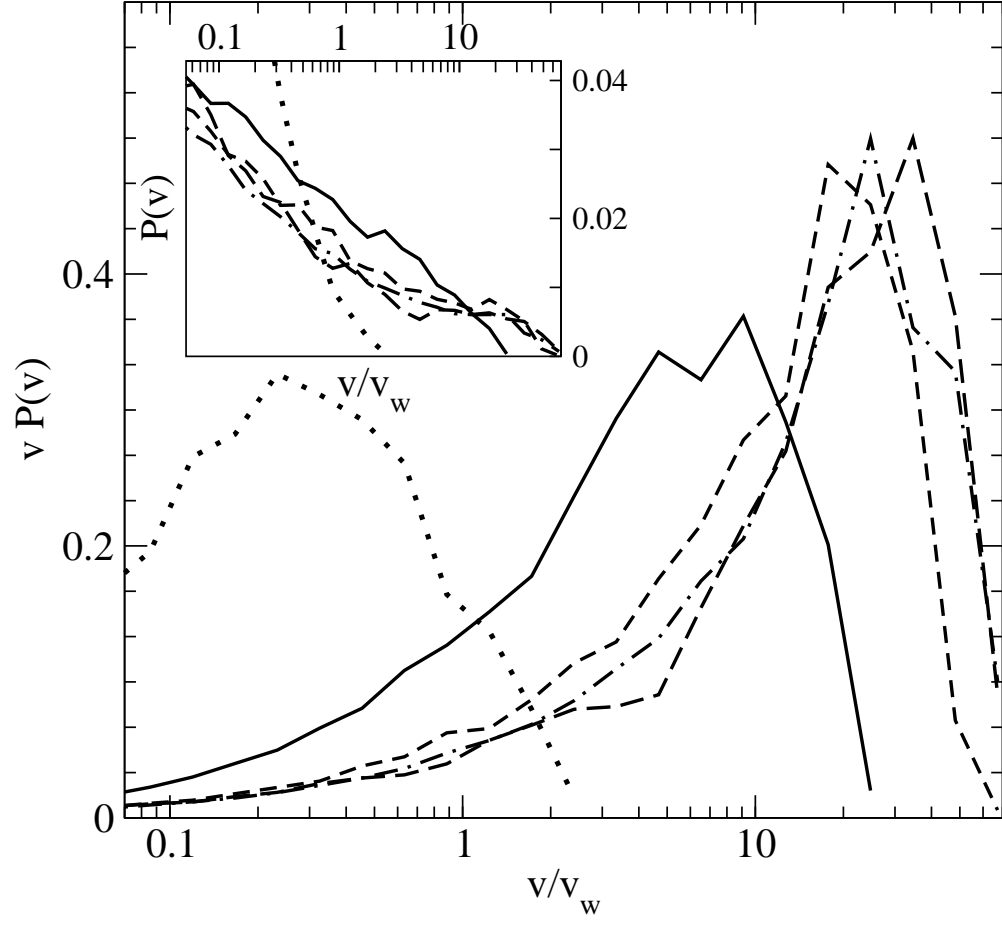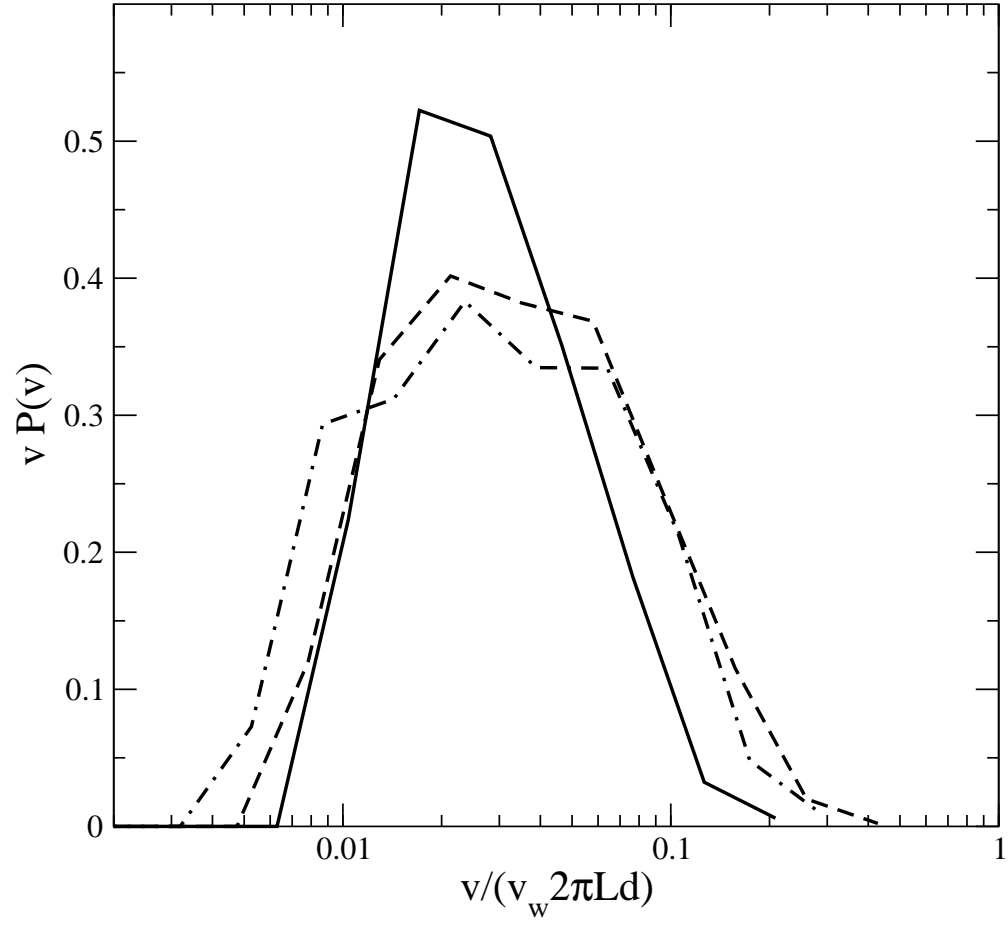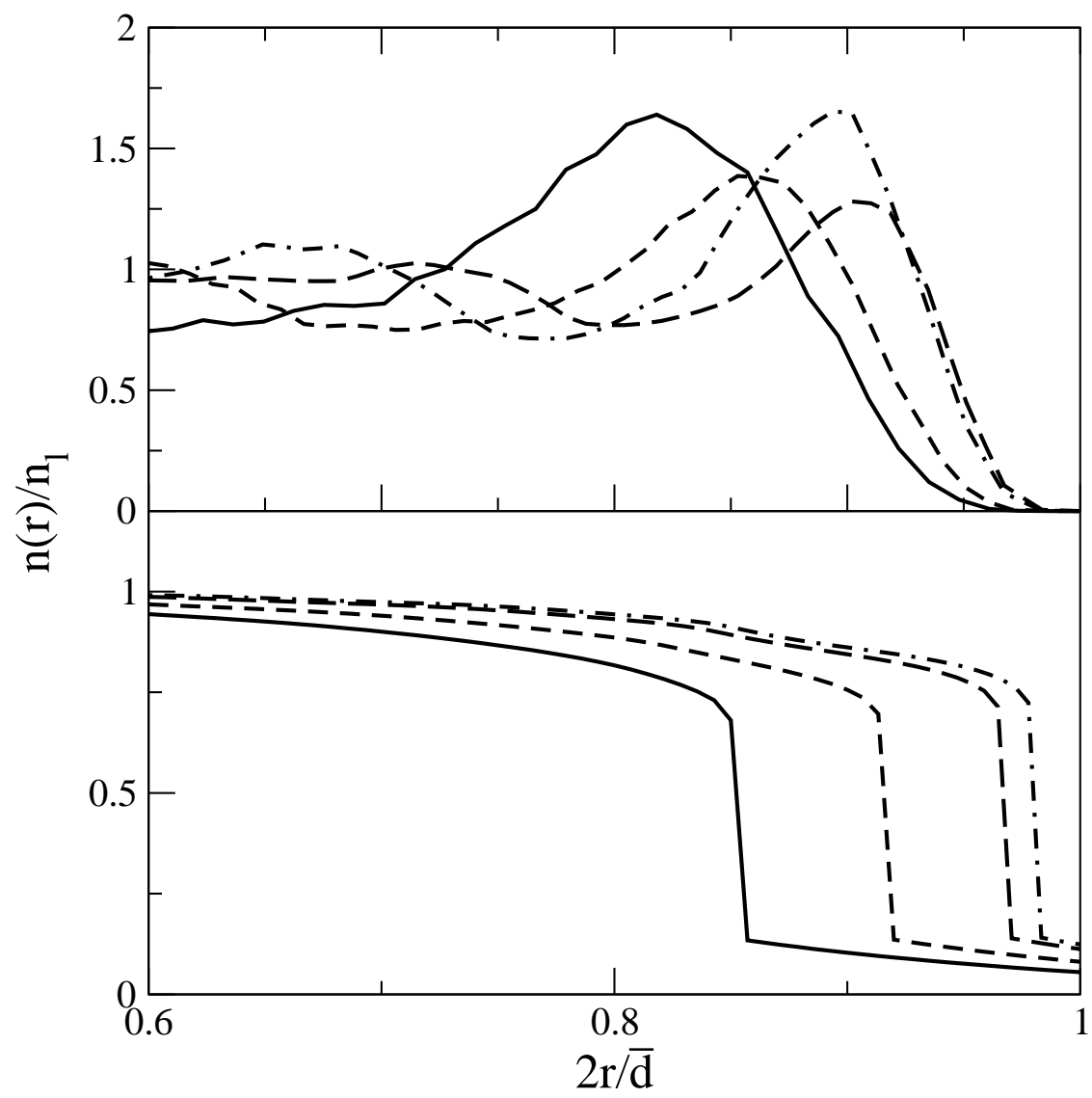
Figure 4, Russo et al.

Figure 5, Russo et al.
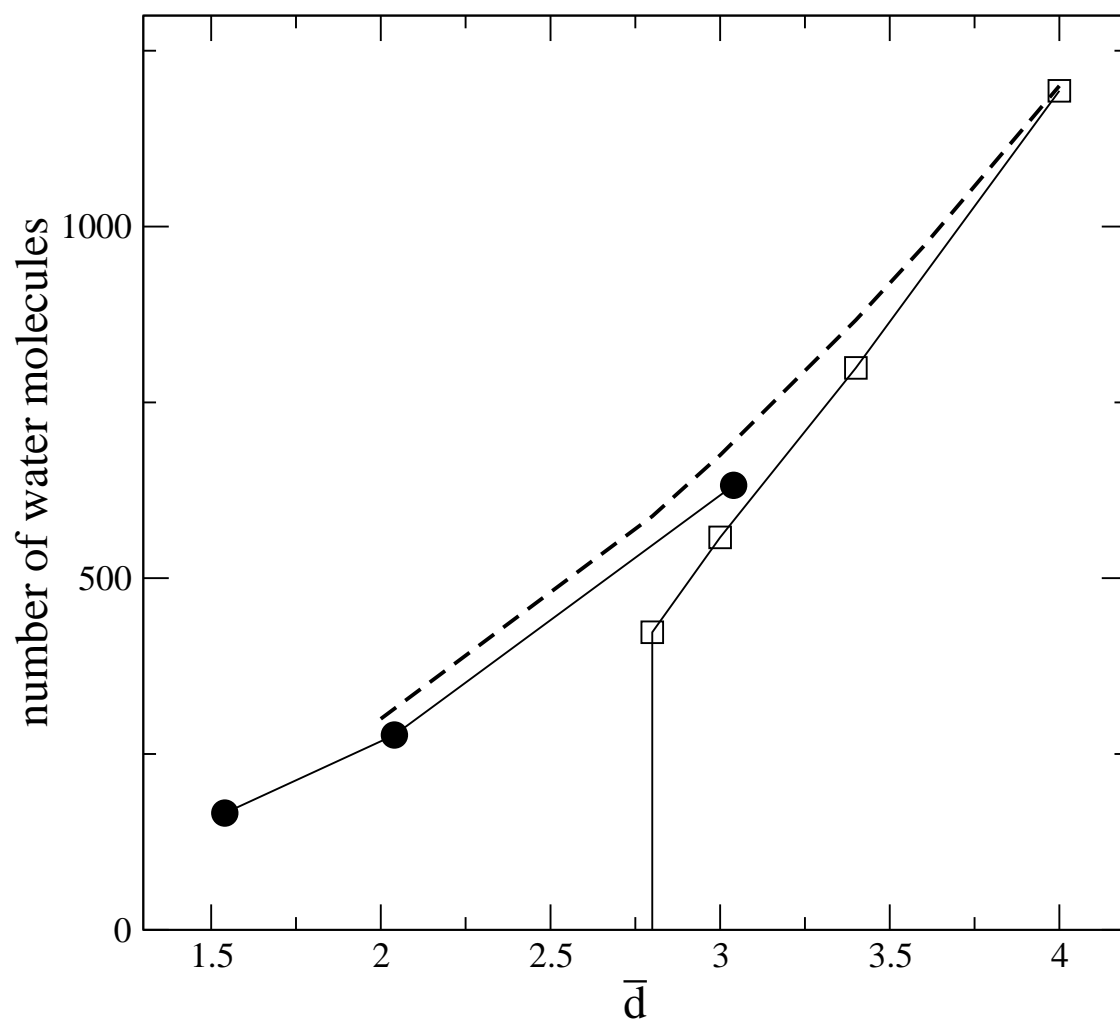
Figure 6, Russo et al.

Figure 7, Russo et al.

Figure 8, Russo et al.